Chemical Communications

COMMUNICATION

Supporting Information

Demonstrating the steady performance of iron oxide composites over 2000 cycles at fast charge-rate for Li-ion batteries

Z. Sun,[a,b] E. Madej,[a] A. Genç,[c] M. Muhler,[e] J. Arbiol,[c,d] W. Schuhmann,[a] and E. Ventosa*[a]*

Experimental Section

Materials

All chemicals used in this work were of analytical grade and used as supplied. Ferrocene was supplied by Sigma-Aldrich (product number F408) and used without further treatments. Commercial iron oxide nanopowders were purchased from Aldrich (product numbers: *a*-Fe_2O_3: 544884; Fe_3O_4: 637106).

Formation of carbon-coated FeO_x/CNTs composites

Typically, 100 mg of ferrocene was added into a 25 ml stainless steel autoclave. The autoclave was flushed with N_2 to remove the air and maintained at 550 or 650 ºC for 2 h. After cooling to 350 ºC, the reactor was opened with caution. The pressure of atmosphere increased to 2 bar at 350 °C, while the overpressure of the residues of the synthesis (typical yield of *ca.* 65 %) is almost negligible.The collected dark sample was subjected to washing with distilled water and absolute ethanol three times to remove excess of remaining ferrocene followed by drying at 60 ºC overnight. Figure S1 shows a schematic illustration of the formation of the composite.

The role of the carbon coating in the electrochemical cycling performance of the composite is more important than that of CNTs since the coating not only increases the electric conductivity but also prevents the pulverization of

iron oxide upon cycling. Therefore, our objective was to promote the carbon coating and minimize the growth of CNTs. Since high temperatures and high flows of carbon precursor should favour the growth of CNTs, the synthesis was conducted at 650 °C (also beneficial for small particle size) or below in absence of flow (in an autoclave).

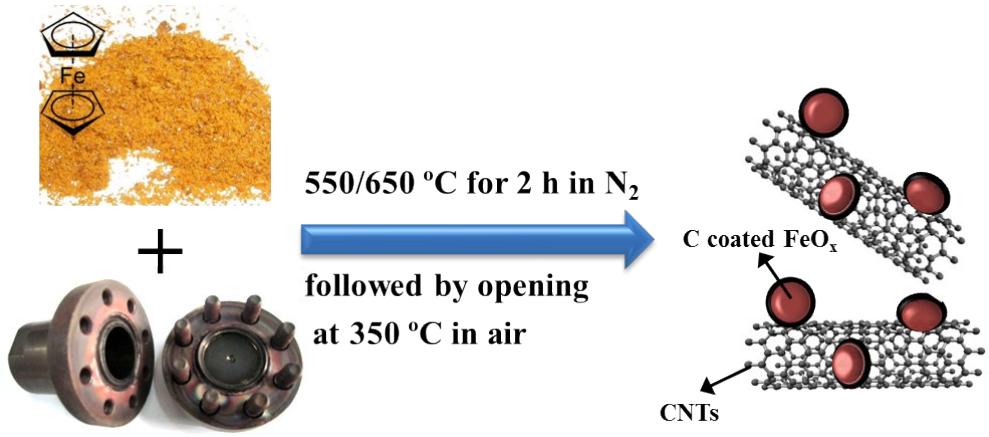

Figure S1. Schematic illustration of the formation of carbon-coated FeOx/CNTs composite.

Structural characterization

Powder X-ray diffraction (XRD) was performed using a PANalytical X'Pert PRO X-ray diffractometer operated at 30 kV and 100 mA with Cu Kα radiation. Simultaneous differential scanning calorimetry (DSC) and thermogravimetric analysis (TGA) (SDT) measure both the heat flows (DSC) and weight changes (TGA) associated with transitions in a material as a function of temperature and time in a controlled atmosphere. SDT was performed using a SDT 2960 instrument in air. X-ray photoelectron spectroscopy (XPS) measurements were carried out on an ESCAL Lab 220i-XL spectrometer operated at 15 kV and 20 mA at a pressure of ~3×10^{-9} mbar using Al Kα as the excitation source (hv = 1486.6 eV). Infrared spectra were recorded in the transmission mode with a resolution of 8 cm^{-1} using a PerkinElmer Spectrum RXI FTIR spectrophotometer equipped with a $LiTaO_3$ detector. Pellets were used for IR measurements which were prepared by pressing the sample in KBr (sample-to-KBr mass ratio of 1 : 1000 in the mixture) under 1.0×10^8 Pa for 2 min. Raman spectra were measured using a Perkin Elmer RamanStation 400F spectrometer that employs laser excitation at 785 nm (1.58 eV) delivering 100 mW. To avoid heating of FeO_x NPs, which are known to easily transform into hematite under laser irradiation at a temperature close to 240 ºC, the nominal laser power was reduced by a filter down to 5 mW. Deposited thin films

were prepared by vacuum filtration of the dispersions in ethanol onto porous nylon membranes (Whatman, 0.2 μm pore size, 47 mm membrane diameter) and dried at room temperature. Measurements were taken with 2 s of exposure time and ~100 nm of beam diameter using a 15 mm working distance objective. The spectra were base line corrected. SEM images were obtained with a field emission microscope (FEI Quanta 600 FEG) operated at 20 kV and equipped with an energy-dispersive X-ray spectrometer (EDX). TEM studies were conducted by using a field emission gun FEI Tecnai F20 microscope operated at 200 kV, which is equipped with a high angle annular dark field (HAADF) detector and Quantum Gatan Image Filter (GIF) for electron energy-loss spectroscopy (EELS) analyses.

Nitrogen adsorption-desorption measurements were performed using a TriStar II (Micromeritics) analyzer to determine the Brunauer-Emmett-Teller (BET) surface area and Barrett-Joyner-Halenda (BJH) pore size distribution. Prior to N_2 adsorption at 77 K, the samples were degassed in vacuum at 110 ºC for 6 h to remove adsorbed and undesired species from the sample surface.

Electrode preparation and electrochemical characterization

Carbon-coated FeO_x/CNTs composites were grinded with a mortar and pestle and then mixed with appropriate amounts of C65 carbon black (Timcal, Bodio) and polyvinylidenedifluoride (PVdF) binder (Solef S5130, Solvay) in NMP. The content of carbon in the composite electrodes was unified by adjusting it with C65 carbon black, and electrodes with the same carbon content (47 %) were prepared from the commercial iron oxides. After exposure to bath ultrasonication for around 6 min, the mixture was cast onto a copper foil using the Doctor-Blade technique and dried at 60 °C overnight. Subsequently, 12 mm disk electrodes were punched out with a commercially available hole puncher (Hoffmann) and were subjected to vacuum-drying at 105 °C for 3 h. The electrode loadings were *ca.* 0.5 mg cm^{-2} and the geometric area of the electrode was 1.13 cm^2. Three-electrode Swagelok cells were assembled in an Ar-filled glovebox (O_2 < 2 ppm and H_2O < 1 ppm). Whatman GF/D glass fiber filters served as separators. LP40 electrolyte (150 mL of 1 M $LiPF_6$ in ethylene carbonate/diethyl carbonate) was purchased from Merck and used as received. Electrochemical impedance spectroscopy (EIS) measurements were performed between 100 kHz – 100 mHz with an amplitude of 10 mV using a specially designed co-axial cell.[1] All electrochemical measurements were carried out using a Bio-Logic VMP-3 potentiostat. Charge/discharge rates of 1000 and 2000

mA g^{-1} were applied during cell cycling within the potential window 3.0–0.1 V. All specific capacities were normalized based on the mass of iron oxides. All potentials are given versus Li/Li^+ in 1 M $LiPF_6$.

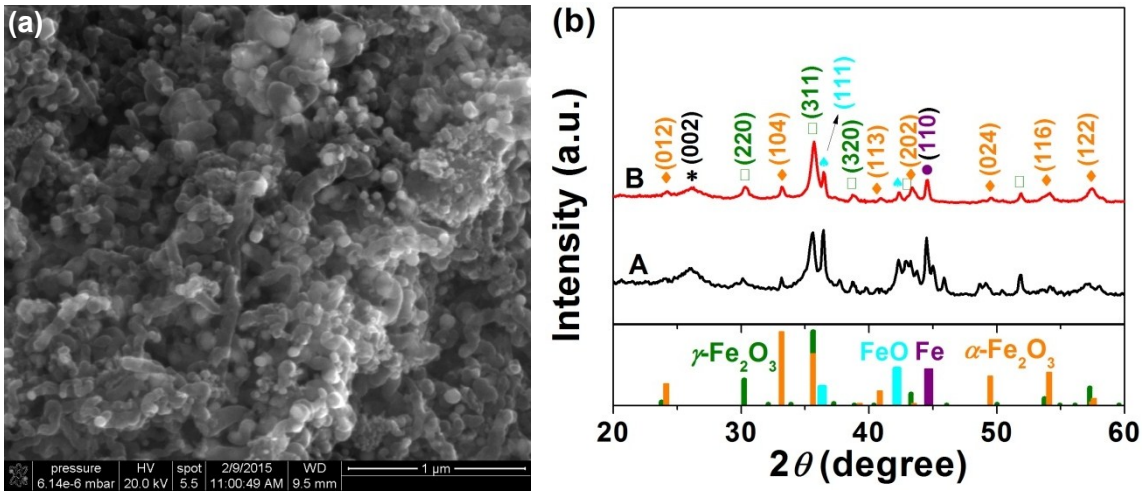

Figure S2. (a) SEM micrograph of FeO_x(550)/C. (b) XRD patterns of FeO_x(550)/C before (trace A) and after annealing (trace B).

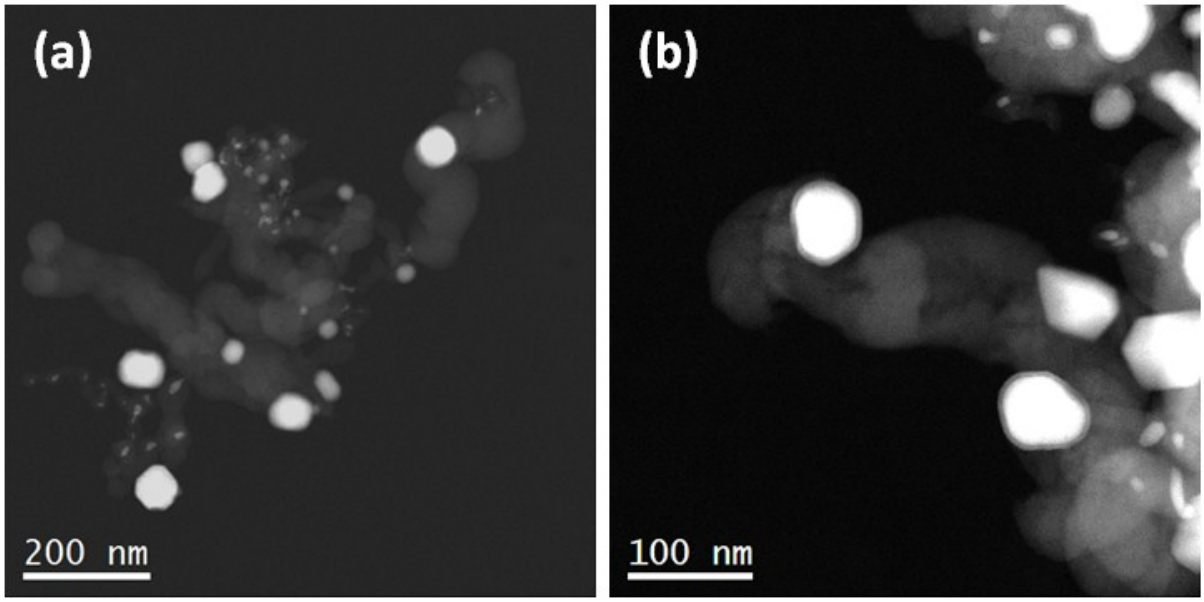

Figure S3. HAADF STEM micrographs of (a) FeO_x(550)/C and (b) FeO_x(650)/C.

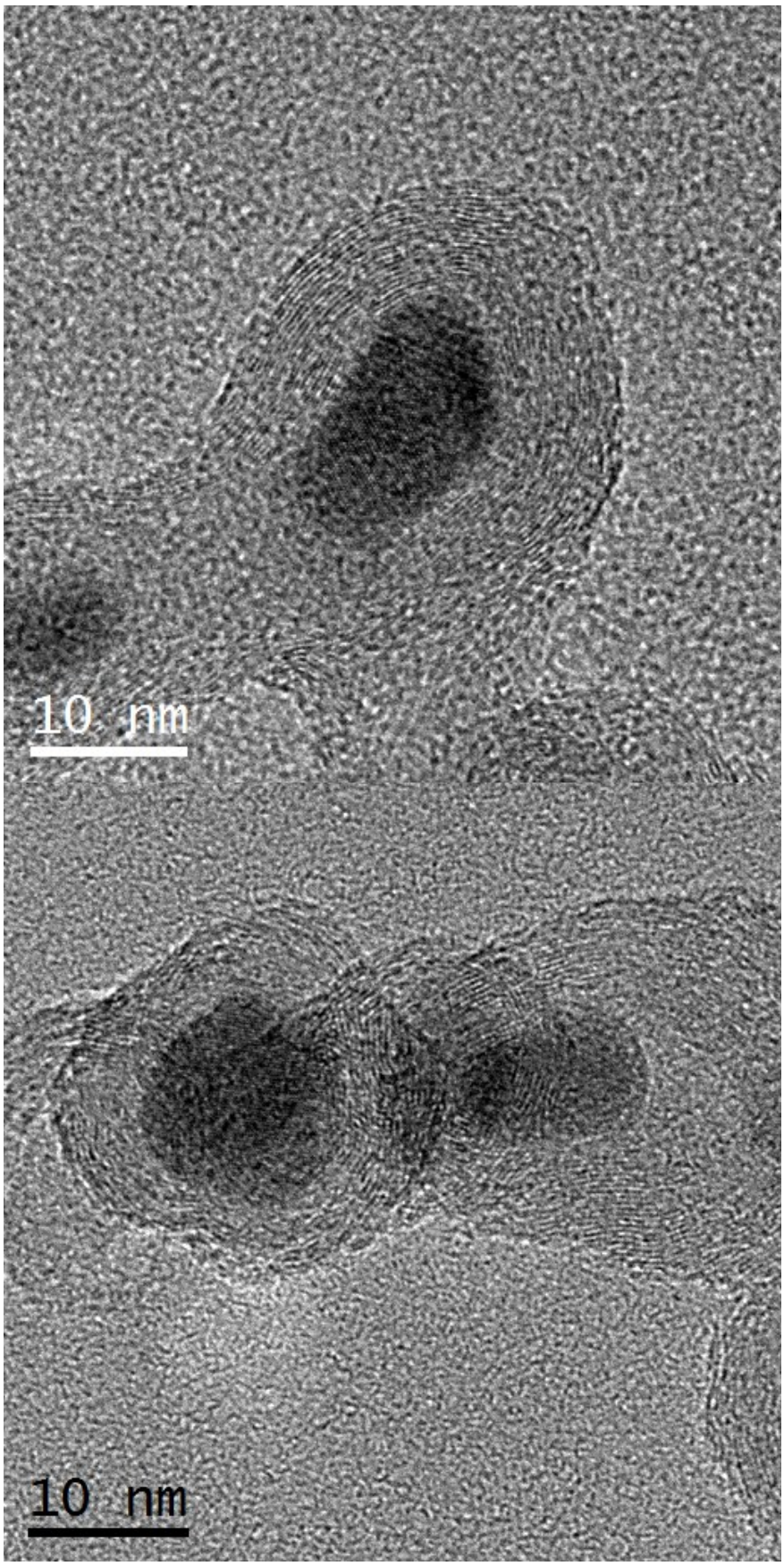

Figure S4. HRTEM micrograph of FeO_x(650)/C.

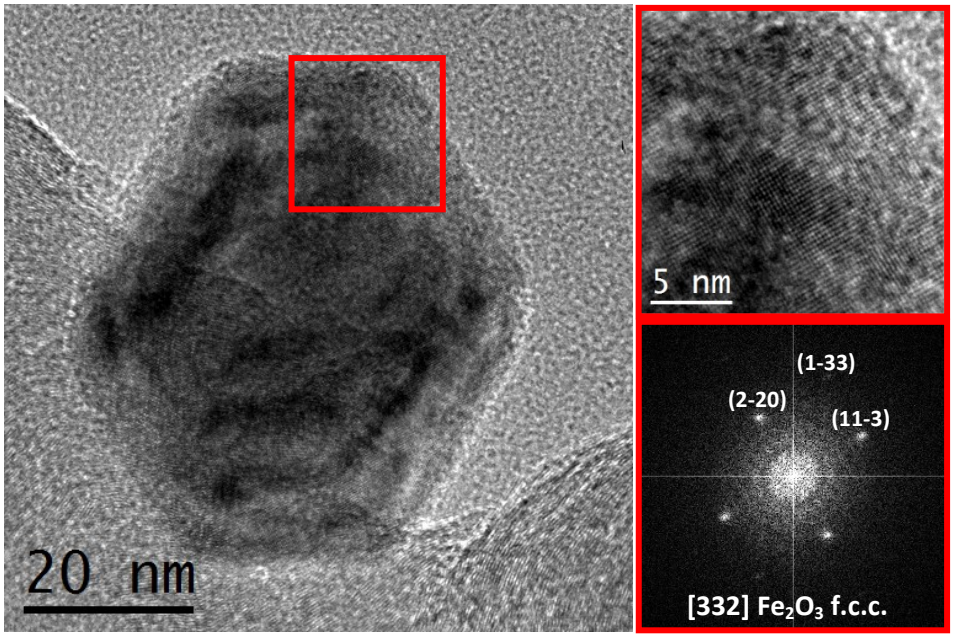

Figure S5: HRTEM micrograph of a hexagonal faceted ~ 50 nm nanoparticle (left), details of the red squared region (top right) and its corresponding power spectrum (bottom right).

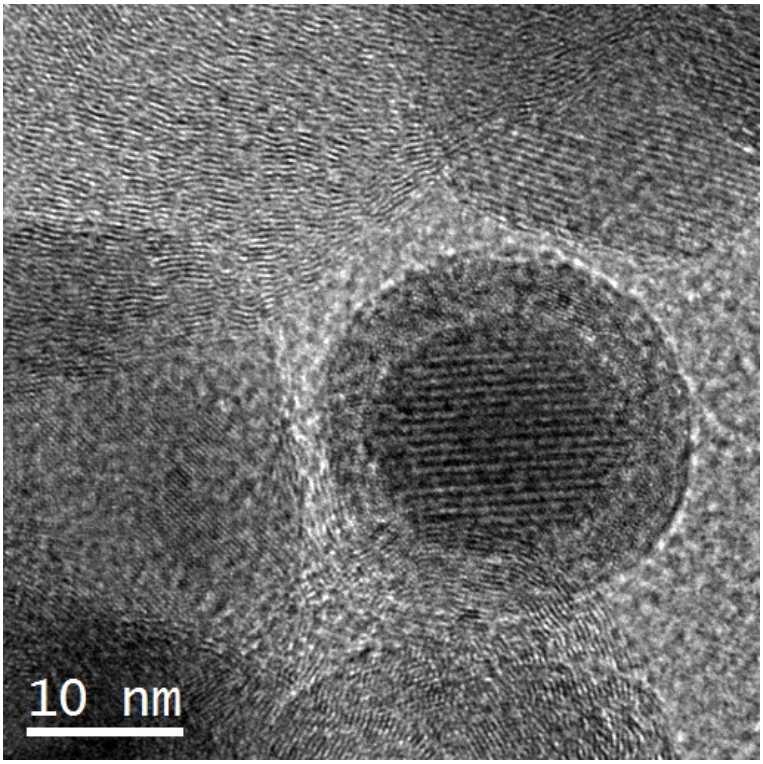

Figure S6: HRTEM micrograph of a spherical ~ 24 nm core-shell nanoparticle with a ~ 4.3 nm thick shell, revealing the presence of Moiré fringes.

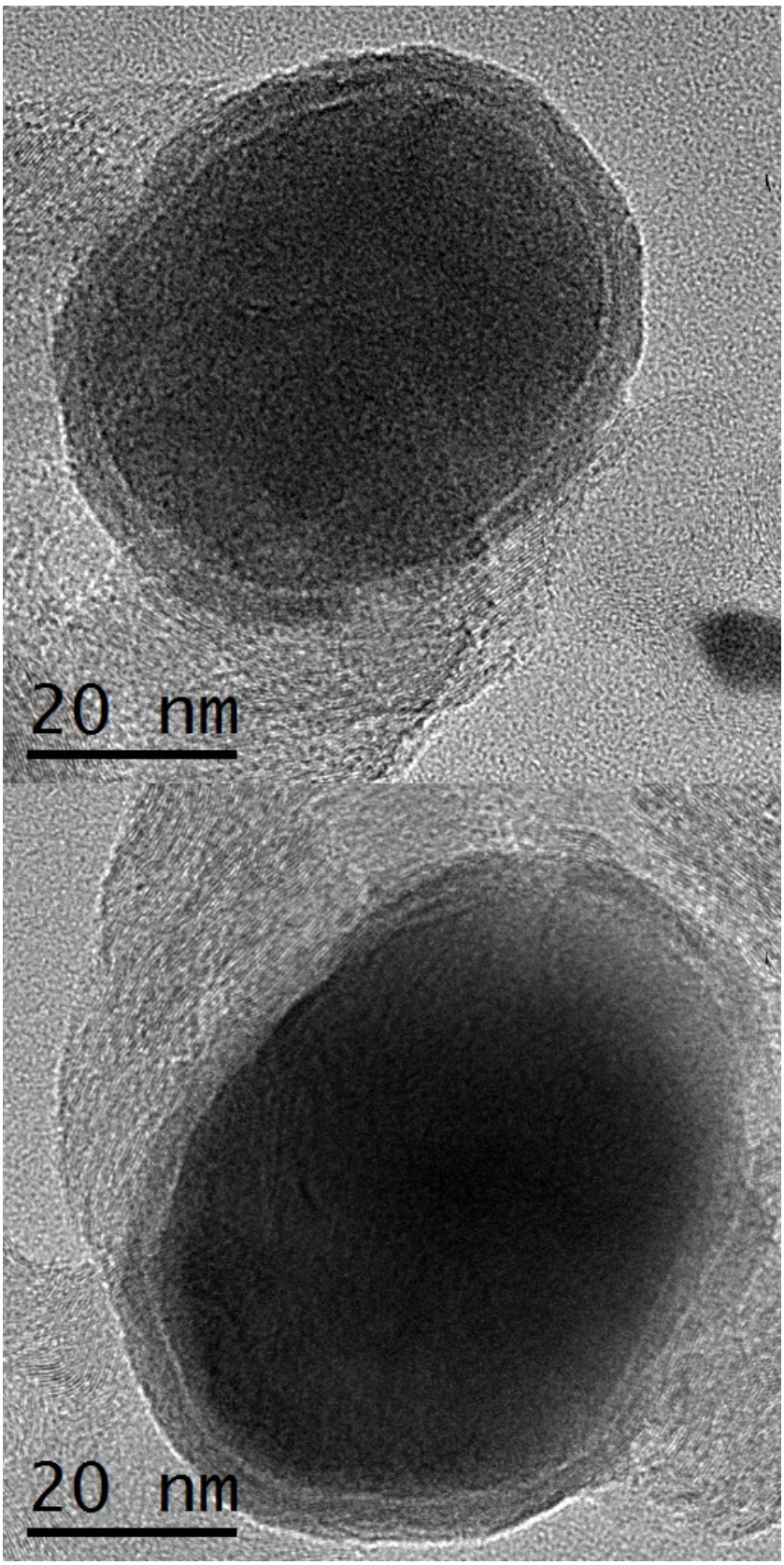

Figure S7: HRTEM micrographs of core-shell nanoparticles acting as catalysts of CNTs.

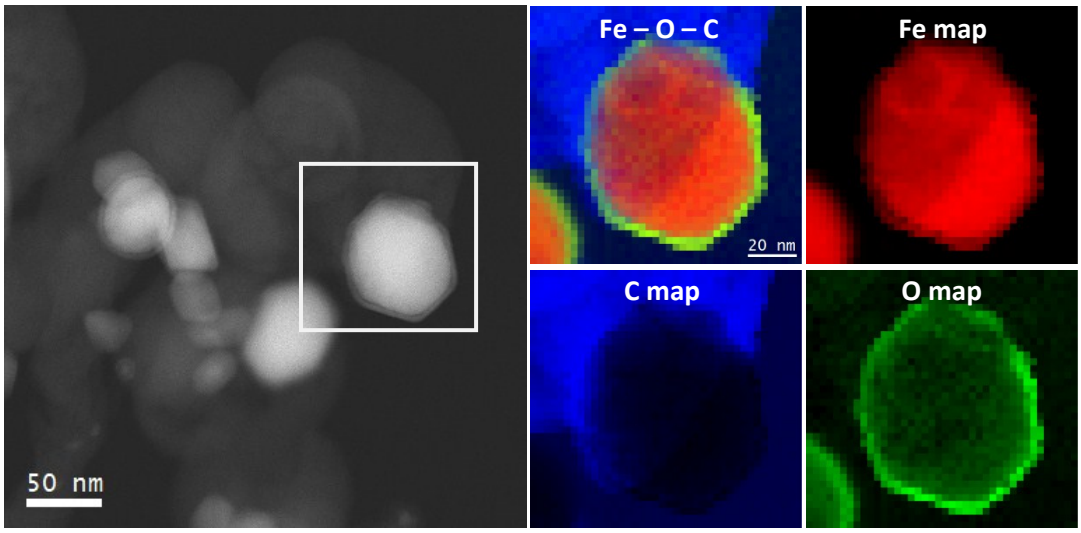

Figure S8: HAADF STEM micrograph showing several nanoparticles in the C matrix and EELS composition maps of the white squared area. Individual Fe (red), O (green) and C (blue) maps along with their composite. Scale bar is the same for all composition maps.

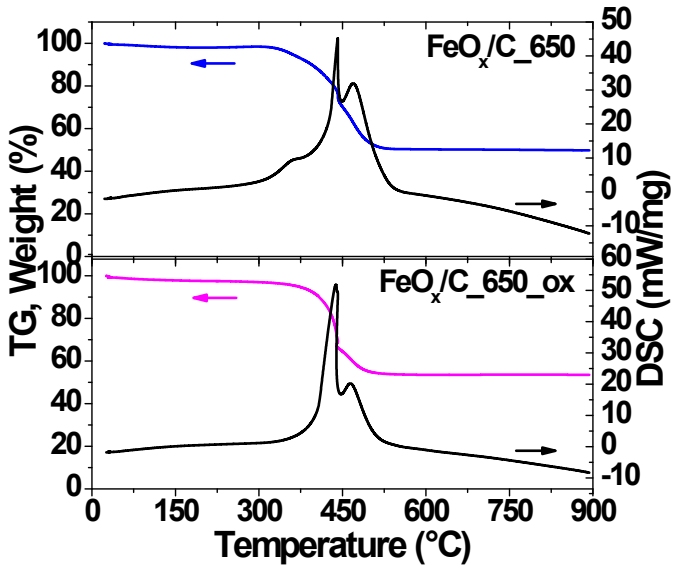

Figure S9. Thermogravimetric (TG) and differential scanning calorimetry (DSC) thermograms for FeO_x(650)/C (top panel) and FeO_x(650)/C_ox (bottom panel), obtained with a ramp rate of 10 °C min^{-1} in air with a flow rate of 100 mL min^{-1}.

A small weight loss <3 wt% prior to 300 ºC for both samples is due to the removal of physically adsorbed water. The two pronounced endothermic peaks at 440 and 470 ºC represent the oxidation of the two C forms in the sample. The latter may also correspond to maghemite to hematite phase transition. (Cornell R.M., Schwertmann U.,

The iron oxides: structure, properties, reactions, occurrences. John Wiley, Cambridge, 2003.) An additional broad peak was observed for FeO_x(650)/C which may be attributable to the loss of trace amounts of amorphous C and/or oxygen-containing groups in the C structure. From the TG thermogram, the FeO_x content was estimated to be around 50 wt% for FeO_x(650)/C_ox, agreeing well with the elemental analysis results.

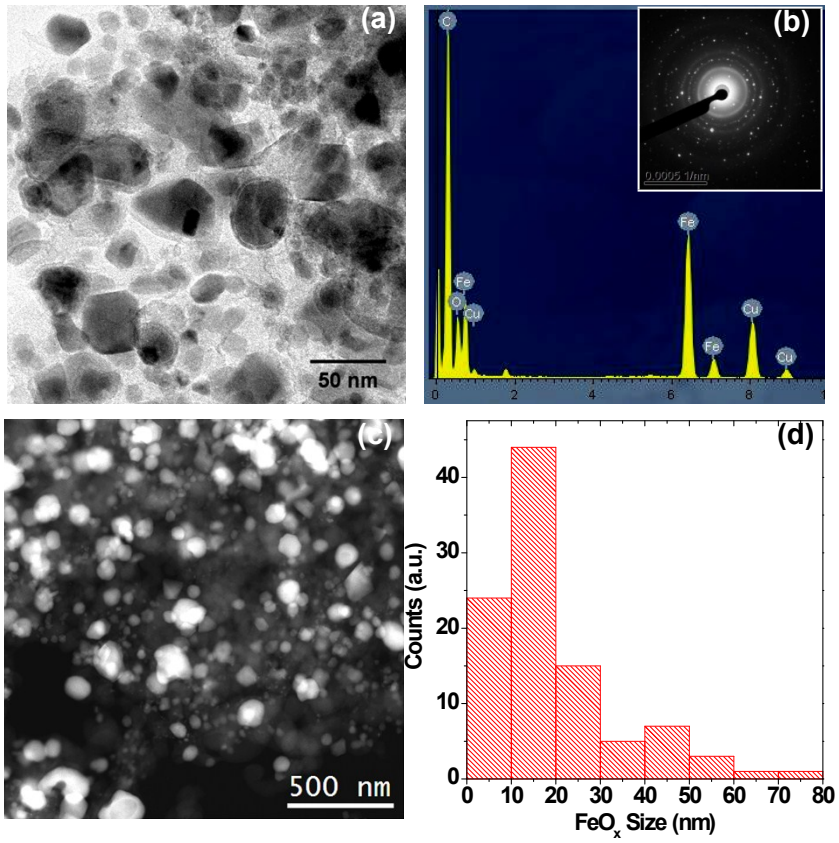

Figure S10. (a) Typical TEM image of FeO_x/C_650 at low magnification. (b) EDX pattern taken from the region in a. Inset: electron diffraction pattern of the sample. (c) STEM image of FeO_x/C_650 at low magnification. (d) Size distribution of FeO_x NPs.

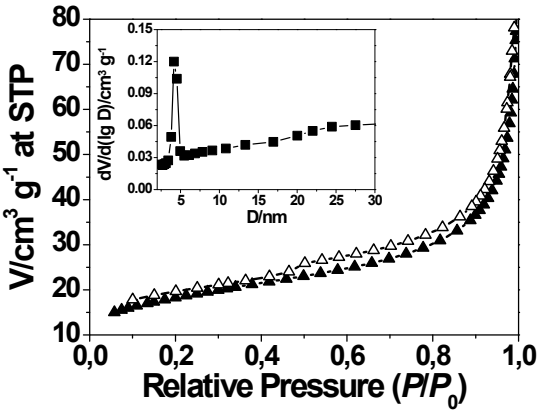

Figure S11. N_2 adsorption/desorption isotherms of FeO_x(650)/C. Inset: pore size distribution calculated from the desorption branch of the isotherms.

As shown in Figure S10, a type II isotherm was observed for FeO_x(650)/C based on nitrogen adsorption/desorption measurements. The gradually increasing adsorption in the relative pressure (P/P_0) range of 0.2-0.3 indicates the mesoporous character. The small adsorption in the P/P_0 range $\leq$ 0.05 is due to some microporosity; the slowly increasing adsorption in the mid-range of P/P_0 originates from multilayer adsorption; and the sharp adsorption/desorption hysteresis loop at P/P_0 > 0.8 related to the mesopores *via* a capillary condensation mechanism. The average BJH (Barrett-Joyner-Halenda) pore diameter (inset of Figure S10) calculated from the desorption branch of the isotherm was estimated to be about 4.2 nm. The BET (Brunauer-Emmett-Teller) surface area was determined as ~ 65.8 $m^2 g^{-1}$ which is significantly higher than those of commercial Fe_3O_4 (~ 40.7 $m^2 g^{-1}$) and α-Fe_2O_3 (~ 37.5 $m^2 g^{-1}$). The high surface area of the as-obtained FeO_x/C with mesoporous structures is beneficial to electrolyte accessibility, rapid Li^+ diffusion and volume accommodation of FeO_x.

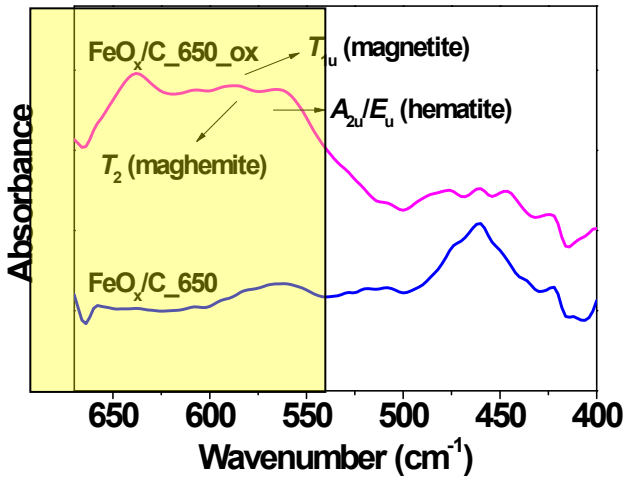

Figure S12. IR transmission spectra of FeO_x(650)/C prior to (bottom) and after (top) calcination in air at 300 ºC.

In both cases, broad absorption peaks were observed in the spectra region 500-660 cm^{-1}, suggesting the combination of T_{1u}, T_2, and A_{2u}/E_u vibrational modes (stretches of Fe-O bonds) of magnetite, maghemite and hematite, respectively. (I. V. Chernyshova, M. F. Hochella Jr and A. S. Maddenc, *Phys. Chem. Chem. Phys.*, 2007, 9, 1736–1750).

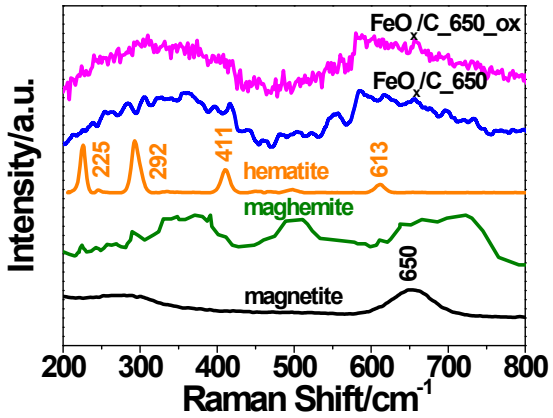

Figure S13. Raman spectra of FeO_x(650)/C before and after calcination in air at 300 ºC (FeO_x(650)/C_ox), and standard hematite, maghemite and magnetite.

The peak at around 506 cm^{-1} can be assigned to the Raman T_{2g} mode of maghemite. The broad peak in the region of 550-750 cm^{-1} may contain E_g (~ 613 cm^{-1}) mode of hematite, A_{1g} modes of maghemite (~ 695 cm^{-1}), magnetite (~

650 cm^{-1}). The peak in the range between 200 and 450 cm^{-1} may encompass A_{1g} (~ 225 cm^{-1}) and E_g (~ 292, ~ 411 cm^{-1}) modes of hematite, and E_g (~ 360 cm^{-1}) mode of maghemite. (T. Sharifi, E. Gracia-Espino, H. R. Barzegar, X. E. Jia, F. Nitze, G. Z. Hu, P. Nordblad, C. W. Tai, T. Wåberg. *Nat. Commun.* 2013, 4, 2319.)

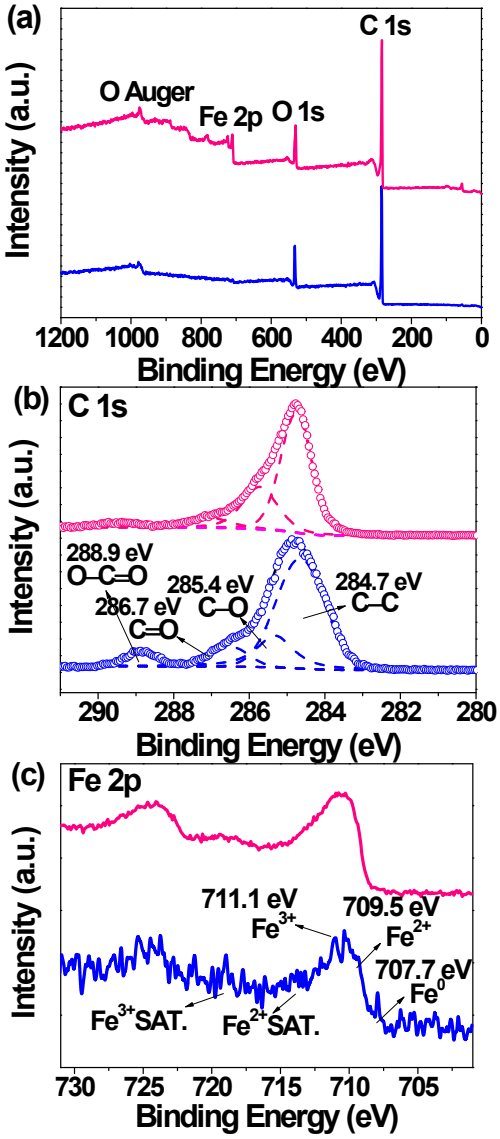

Figure S14. (a) Wide-survey, (b) C 1s and (c) Fe 2p XPS spectra of FeO_x(650)/C before (bottom, in blue) and after annealing (top, in purple, FeO_x(650)/C_ox).

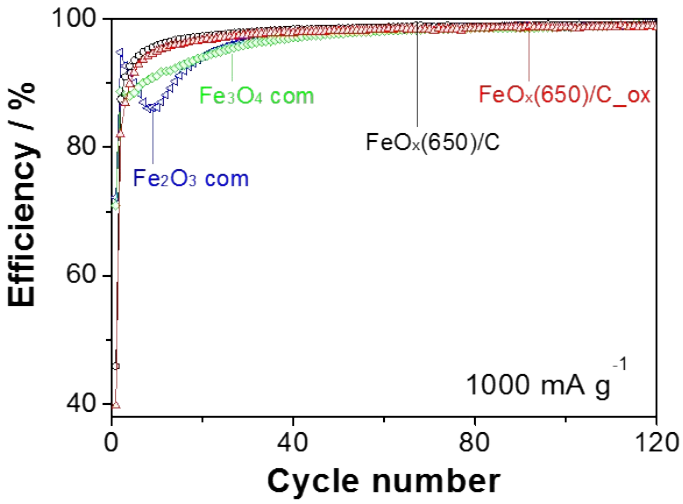

Figure S15. Coulombic efficiency of commercial Fe_2O_3, Fe_3O_4, $FeO_x(650)/C$ and $FeO_x(650)/C\_ox$ at 1000 mAh g^{-1} in the potential range 3.0 – 0.1 V vs. Li/Li^+.

Figure S16 shows the Nyquist plots from the EIS measurements of commercial Fe_2O_3, Fe_3O_4 and $FeO_x(650)/C\_ox$ recorded at ca. 50 % state of charge (SOC) in the (a) 1st cycle and (b) 51st cycle. While the charge transfer resistance associated to the size of the semi-arc drastically increased after 50 cycles for commercial samples, it remained constant for $FeO_x(650)/C\_ox$, even slightly decreased. During the conversion reaction, iron oxide particles convert into metallic iron with a surrounding film of Li_2O. Because of the insulating character of Li_2O as well as the large volume changes during the conversion reaction, particles may lose the electric contract to the rest of the electrode (particle decohesion), which can be referred to as degradation of the electrode. The higher impedances observed for the commercial samples after cycling indicate a severe degradation of the electrode. On the other hand, the impedance did not increase upon cycling for the composite showing good integrity of the electrode. There are two intriguing features in the EIS results of $FeO_x(650)/C\_ox$. I) No middle frequencies semi-arc associated with the SEI was observed and II) the impedance slightly decreased upon the first 50 cycles. The former is likely due to the cutoff potential of 0.1 V vs. Li/Li+ which prevents the formation of thick SEI. The latter is likely due to the major structural re-organization occurring during the first cycle. The particles are split into smaller metallic nuclei, and the initial structure is not recovered during the reverse process. As a consequence, the first cycle always shows slightly different electrochemical features than those of the subsequent cycles, e.g. lower cathodic plateau. This restructuring requires some additional energy which may explain the slightly higher impedance of the first cycle.

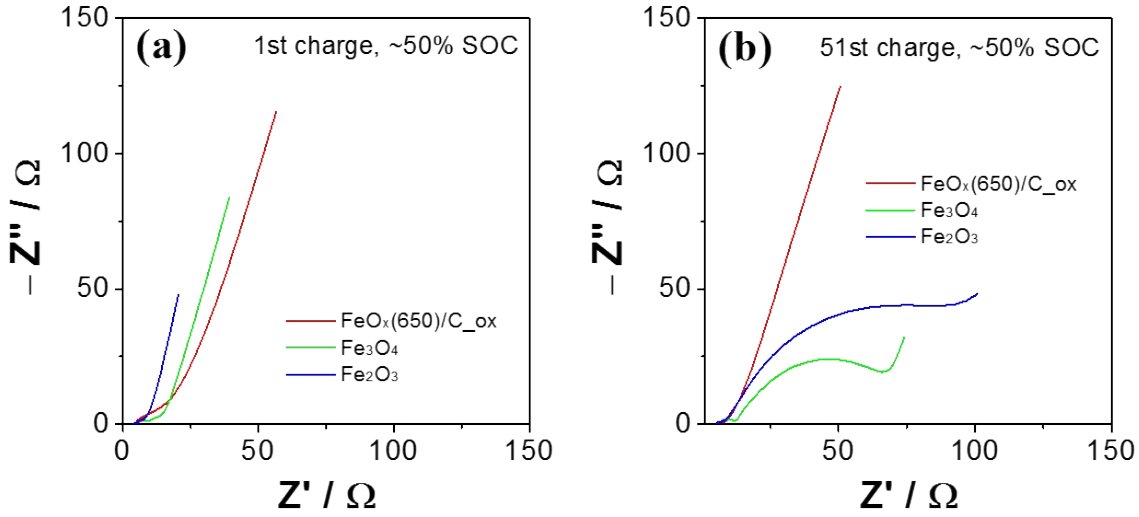

Figure S16. Electrochemical impedance spectroscopy (EIS) spectra for commercial Fe_2O_3, Fe_3O_4 and FeO_x(650)/C composite recorded at ~0.8 V during a) cycle 1, and b) cycle 51.

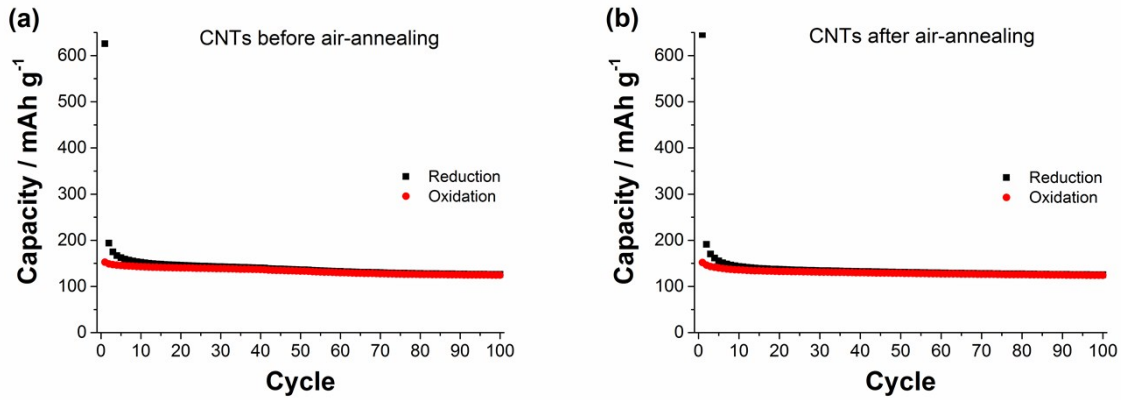

Figure S17. Electrochemical performance of commercial CNTs (a) as-received and (b) air-annealed, at 2000 mA g^{-1} in the potential range 3.0 – 0.1 V vs. Li/Li^+.

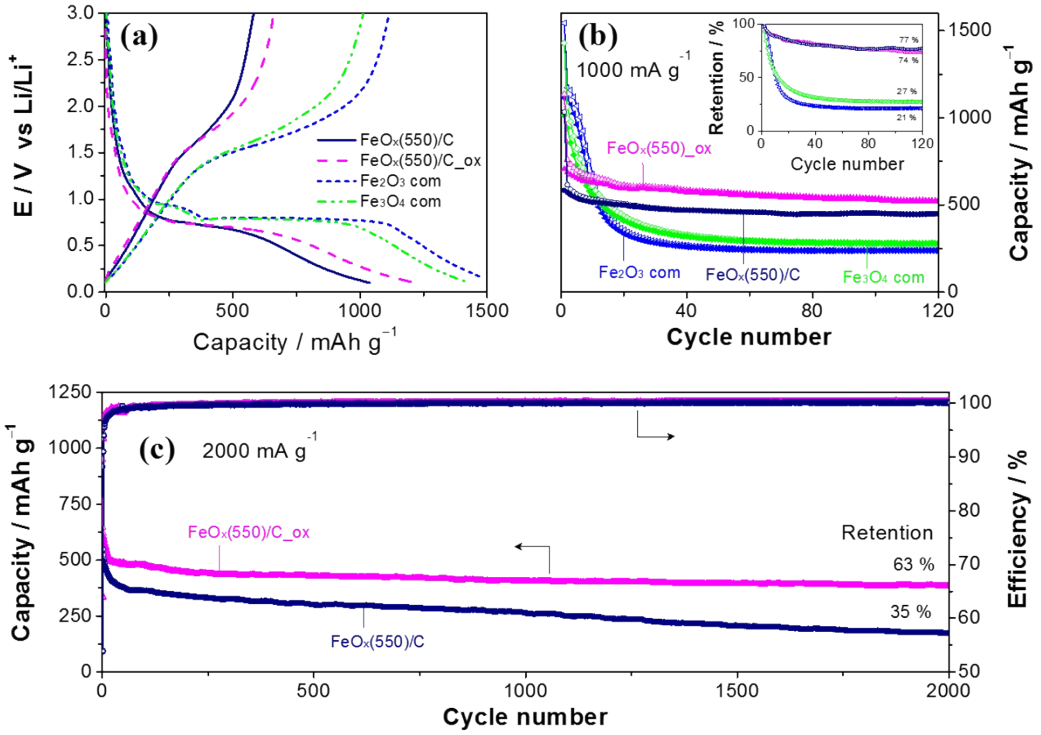

Figure S18. Electrochemical characterization of commercial Fe_2O_3, Fe_3O_4, FeO_x(550)/C and FeO_x(550)/C_ox.

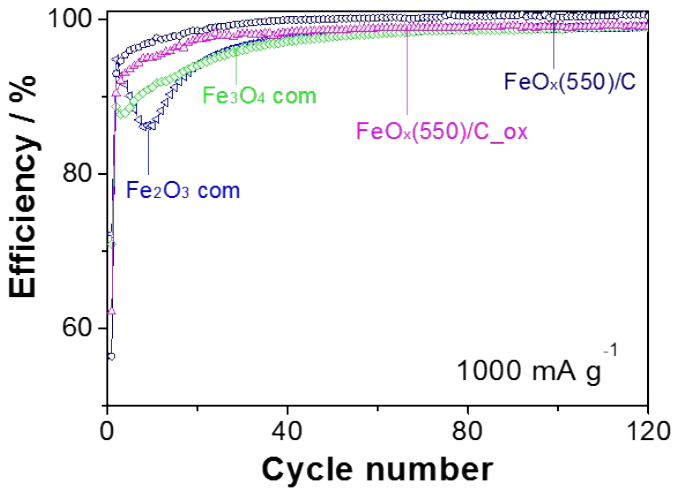

Figure S19. Coulombic efficiency of commercial Fe_2O_3, Fe_3O_4, FeO_x(550)/C and FeO_x(550)/C_ox at 1000 mAh g^{-1} in the potential range 3.0 – 0.1 V vs. Li/Li^+.

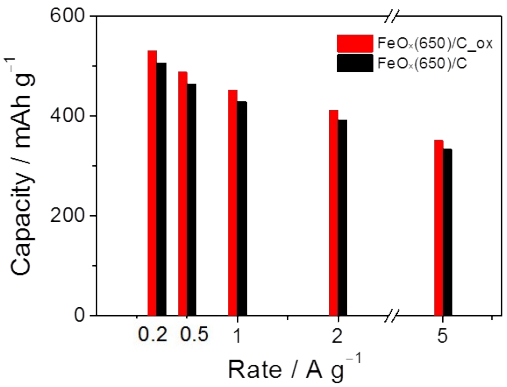

Figure S20. C-rate performance of FeO_x(650)/C_ox at 0.5 C, 1 C, 2 C, 4 C and 10 C (0.2, 0.5, 1, 2 and 5 A g-1, respectively) in the potential range 3.0 – 0.1 V vs. Li/Li^+ carried out after prolonged cycling.

Electrochemical determination of X in FeO_x.

It is not possible to reliably determine "x" in FeOx for our samples. In a carbon-free iron oxide sample, temperature programmed reduction (TPR) could shed some quantitative light into it. In our samples, some nanoparticles are "protected" by a carbon coating, which hinder the reduction of the core. In addition, there are surface groups at the carbon which will also be reduced during TPR leading to false values in the oxidation state of Fe.

Interestingly, electrochemistry can provide a rough estimation. When cycled at low C-rates, the initial anodic specific charge can be used to make a rough estimation of the state of oxidation of Fe. The specific charge (C) of FeOx is given by $C = 2X * F / MWFeOx$, where 2X is the state of oxidation (number of exchanged electrons), F is the Faradaic constant and MWFeOx is the molecular weight of FeOx ($55.85 + X * 16$ moles g^{-1}). Rearranging the equation, gives $X = 55.85\ C / (2\ F - 16\ C)$. After long term electrochemical cycling, the C-rate was decreased down to 0.5 C resulting in a reversible capacity of around 550 mAh g^{-1}. According to the equation, the effective X value is 0.63, which means that the average state of oxidation of Fe is +1.25.

References

1. S. Klink, E. Madej, E.Ventosa, A. Lindner, W. Schuhmann and F. La Mantia, *Electrochem. Comm.* 2012, **22**, 120

